# Experimental Design to Characterize the Interface of Flexible Hybrid Electronics under Mixed-Mode Fracture

Sara Najafian, Alireza V. Amirkhizi, Scott E. Stapleton

Mechanical Engineering, University of Massachusetts Lowell, Lowell, MA, 01854

***Abstract***: *Flexible Hybrid Electronics (FHEs) are finding increasing applications since they overcome the limitations of rigid and non-deformable traditional electronic boards and circuits. A key parameter in FHE performance is the adhesion of printed conductive silver pastes to the flexible substrate. Prediction of the failure mechanism of the interface, under large deformations and with a considerable material mismatch, is fundamental to future design efforts. However, due to the complex nonlinear behavior of the materials and size of components, common interfacial characterization tests may not always be feasible. Therefore, numerical models are implemented to design new interfacial characterization experiments. To implement a Cohesive Zone surface model at the interface, a traction-separation relationship is needed to characterize the interface. In this study, a biaxial loading configuration was designed to extract the mixed mode traction-separation parameters. The sensitivity of the mixed-mode ratio to the biaxial loading ratio was measured through a parametric study. The results have shown that the specimens can capture a wide range of mixed-mode ratios by changing the biaxial loading configuration. The extracted parameters for the traction-separation relation will be used for future reliability analysis of FHEs under complex loading conditions.*

***Keywords***: *Flexible, Interface, Characterization, Cohesive Zone, Traction-Separation, Mixed-Mode*

## 1. Introduction

Flexible Hybrid Electronics (FHEs) are finding increased popularity over common rigid circuit boards(Leenen et al., 2009). FHEs are the new generation of electronics combining flexible plastic film substrates with electronic devices. The ability to withstand large mechanical deformation results in a vast range of applications for FHEs. Therefore, understanding the capability of these devices under twisting, bending and stretching will improve the functionality of FHEs in fields such as bio (Dagdeviren et al., 2014; Kim et al., 2012), consumer electronic devices and high-tech industries. However, the mismatch of material behavior between the flexible substrate and the printed circuit can lead to complex mechanical behavior at the interface under various loading conditions. Therefore, it is of paramount importance to identify the crucial failure mechanisms. Interfacial failures are one of the most common and difficult failures in FHEs (Park et al., 2008; Suo and Hutchinson, 1990). Dissimilar thickness and material properties of FHE components cause a mixed-mode loading, and mixed-mode failure criterion are required (Harris et al., 2016; Van Der Sluis et al., 2010). To address interfacial failure, Linear Elastic Fracture Mechanics (LEFM) was first used by Williams (Williams, 1959) to solve crack problems between dissimilar materials and Hutchinson et al. (Hutchinson and Suo, 1991) characterized the interfacial parameters in layered structures. However, the LEFM approach involves components with linear properties, and limitation arises with inelastic materials. Cohesive Zone Models (CZMs) first proposed by (Barenblatt, 1962; Dugdale, 1960), are able to account for nonlinear behavior of materials at an interface. CZM implementation depends on the determination of a traction-separation law and a proper description of behavior under multi-axial loading. In CZMs, It is assumed that surfaces are held together by cohesive traction. The associated traction-separation law consists of an elastic response before the damage initiation and the softening response because of the damage evolution. Damage is initiated by reaching the maximum surface traction that can be held by the interface. Damage evolution is represented by the surface traction decrease and quantified by the critical energy release rate, which is the area underneath the traction-separation curve as shown in Figure 2 (Li et al., 2006, 2005).


a) b)

**Figure 1 a) Schematic view of fracture mode: the normal or mode I, and the shear or mode II and b) schematic view of traction separation, where $\sigma_c$ is the maximum stress and $G_c$ is the critical fracture energy.**

Experimental tests are required to obtain the traction-separation law for each fracture mode. The most common tests to extract mode-I and mode-II parameters are Double Cantilever Beam (DCB) and End Notch Flexure (ENF) tests (Kanninen, 1973; Williams, 1989). However, due to the thin and flexible nature of FHEs, manufacturing and testing of either tests is challenging. Different studies have been conducted to determine the correct traction-separation law for mixed-mode failures (Benzeggagh and Kenane, 1996; Cao et al., 2016; Williams, 1989; Wu et al., 2017). Wu et al. obtain mixed-mode traction separation for phase angles from -42° to 0° by changing the adhesive thickness in the End-Loaded Split (ELS) test and combine it with DCB experiments, and the LEFM method was used to calculate the fracture toughness curve (Wu et al., 2016). However, in practice, obtaining the traction-separation parameters can be challenging and time-consuming. Therefore, investigating the failure mechanism of a parametrized shape by a numerical model will allow designing the experiments to characterize the interface properties of thin, flexible specimens.

This paper explores the interfacial behavior between printed silver paste and a thin plastic substrate. Numerical models using the commercial software Abaqus were implemented to analyze the failure mechanism. A 2D finite element model was designed to analyze the mixed-mode sensitivity of the model. A Hyperlastic material model were used to model the substrate. Since modeling of hyperelastic material depends on obtaining the material behavior under axial and multiaxial loading conditions, axial and multi-axial experiments were conducted to obtain the constituive model. Additionally, The contact modeled using cohesive surface interaction and the mixed-mode ratio was determined numerically at the contact tip, for different loading conditions. The initial model was under tension as illustrated in Figure 2. Due to the axial tension, the model starts bending in the middle because of the eccentric load path between the two layers. Moreover, because of the Poisson's effect, the paste and the substrate become thinner, which results in an additional mixing of modes. Therefore, to alter the mixed-mode ratio, transverse loading was applied to the model. It was observed that the mixed-mode ratio can be changed by altering the applied transverse displacment.

The paper is organized as follow: Sec. 2.1 describes the experimental setup to obtain the material properties and Sec. **Error! Reference source not found.** provides the computational methods used for modeling. The experimental results are discussed in Sec. 2.3 and the obtained constitute model is described in Sec. 2.4. Moreover, the mixed-mode sensitivity to the loading configuration is reported in Sec. 2.5 and concluded in Sec. 4.

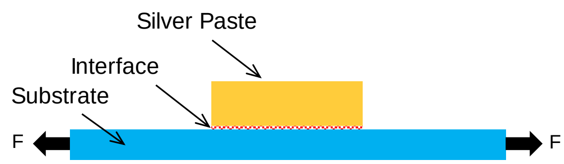


**Figure 2 Schematic view of the 2D model under tension, the adhesive modeled using cohesive surface interaction.**

# 2. Methods

## 2.1 Experiments

### 2.1.1. Materials

Silver paste material properties were taken from literature for a similar paste based on tensile test results (Mu et al., 2017). Since the mechanical properties of the paste are highly dependent on the curing temperature and curing time, the properties were estimated based on the curing temperature and time recommended by the manufacturer and given in Table 1.

**Table 1 Mechanical properties of silver paste (Mu et al., 2017).**

| | Young's modulus (MPa) | Yield strength (MPa) | Yield Strain (%) |
|---|---|---|---|
| **Silver Paste** | 280 | 8.5 | 3.5 |

The following sections outline the details about the experiments to characterize the substrate's material properties. The substrate for this study was Kapton HPP-ST from Dupont which is a two-sided, treated film with a thickness of 75 μm. To characterize the material properties and obtain the constitutive model, uniaxial and equi-biaxial tests were conducted.

### 2.1.2. Uniaxial test

("Standard Test Method for Tensile Properties of Thin Plastic Sheeting," 2012)The first test to characterize the substrate was the uniaxial tension test. Specimens were cut in a rectangular shape with a length of 45 and width of 5 mm. The gauge area was 5x10 mm as shown in Figure 3. The uniaxial test was performed using Electroforce 3200 testing frame from TA instrument and a 400 N load cell. Crosshead displacement was measured using the extended shaft and the force measured by the load cell on the upper axial shaft. Specimens were tested at ambient conditions and the displacement rate was defined as per ASTM D882 ("Standard Test Method for Tensile Properties of Thin Plastic Sheeting," 2012) The displacement rate was 0.05 mm/sec which is equivalent to a strain rate of 0.002 $s^{-1}$.

### 2.1.3. Equi-biaxial test

To obtain the substrate mechanical behavior under multi axial conditions, the substrate was subjected to an equi-biaxial tensile test. The test was performed using the Biaxial Test Bench from TA Instrument. This machine has four actuator arms which can move independently and stretch the specimen in two directions. Because there is no standard which defines the geometry of thin film specimens, a simple geometry was designed to allow a nearly homogeneous stress-strain distribution in the measurement area. Test specimen were prepared by cutting a 34x34 mm square piece of Kapton HPP-ST. The specimen was gripped uniformly during the test and the grip area designed to be 14x10 mm as illustrated in Figure 4a. The force was measured using a 200 N load cell at the end of each actuator arm in each direction. Crosshead displacement was measured based on displacement of each arm. (Figure 4b). The tests were performed at ambient conditions with the same strain rate as the uniaxial test.

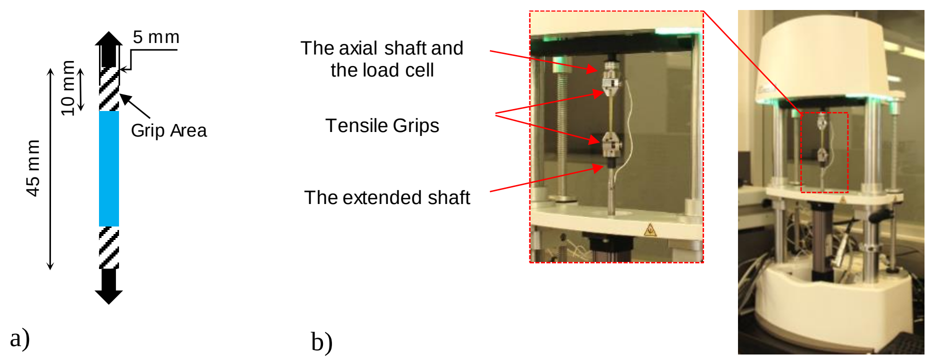


**Figure 3 Uniaxial tensile test of Kapton HPP-ST: a) schematic of the specimen geometry and the grip area b) uniaxial tensile test machine, showing extended shaft, and the load cell at the end of the top axial shaft.**

## 2.2 Numerical methods

The high flexibility and thin geometry of the FHEs caused complexity in interface characterization experiments. Another limitation in designing the experiment was the thin and fragile nature of the silver paste which cannot be easily gripped. Therefore, to predict some of the experimental difficulties and overcome them by changing the design, a 2D finite element model was used to analyze the failure mechanism of the interface using the commercial software Abaqus ("Abaqus Analysis User's Guide (2016),"). The specimen geometry and size were obtained as per the previous study about the effect of the geometry on the mixed-mode ratio (Najafian et al., 2018). Half of the geometry was modeled due to symmetry, as shown in Figure 5a. The substrate was model as a hyperelastic material, and the details of the constitutive model will be discussed in the following section. The silver paste was modeled using an elastic-plastic material model and the properties are given in Table 1. Solid elements (CPS4R) were used, and a nominal element size of 0.03 mm was used as can be seen in Figure 5b. The model was subjected to both axial and transverse displacement. The substrate was stretched on either side as shown in Figure 5b. Since gripping the silver paste was not an option, a compressive displacement was applied to the paste surface and the same area under the substrate and defined as $u_2$ to be able to alter the mixed-mode ratio at the interface.

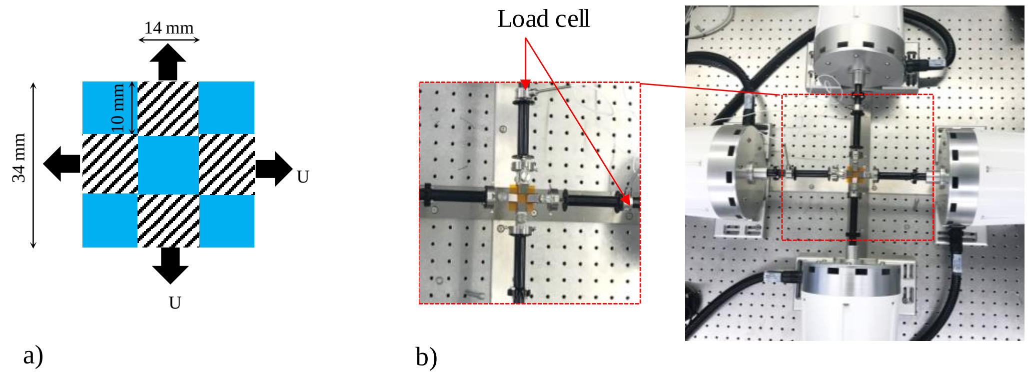


**Figure 4 Biaxial test of Kapton HPP-ST: a) schematic of biaxial specimen geometry b) biaxial planar test bench, consisting of four independent motors, and two load cells for force measurement in two directions.**

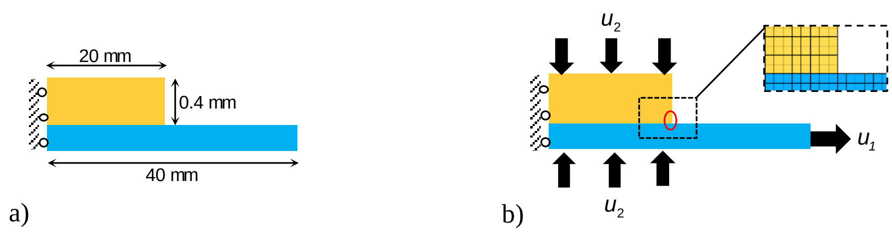


**Figure 5 a) Schematic view of the symmetric model used for finite element modeling and b) the model under transverse and axial displacement**

The interface was modeled using the cohesive surface interaction to predict the failure mechanism based on the traction-separation law parameters. The traction separation parameters included the element stiffness, damage initiation and evolutions. Since the actual damage variables are unknown for this material combination, they were set high enough to avoid fracture during the simulation to be able to investigate the loading effects on the mixed-mode ratio. Therefore, the failure analysis is based on the linear part of the traction-separation law before the damage initiation peak (Figure 1). The linear response before the damage initiation had a stiffness $5.7 \times 10^{14}$

N/m$^3$, and was the same for mode I and II. The maximum stress and critical fracture energy for mode I and mode II were set to 200 MPa, and 80 N/mm, respectively, though as stated before all these values including stiffness were fictitious and inflated to avoid damage. The mixed-mode ratio was defined as the normal to shear stress ratio at the contact tip, $\sigma_n/\sigma_s$ as shown in Figure 5b. Result and discussions

The following sections reports the experimental uniaxial and equi-biaxial results as well as the constitutive model for the material. Additionally, the variation of the mixed-mode ratio with the loading configuration based on the finite element simulation is analyzed.

## 2.3 Experimental results

### 3.1.1. Uniaxial test

Specimens were stretched to failure in the uniaxial tensile test. Ten specimens were tested, although only three specimens did not slip in the grips. Specimens exhibiting slipping in the grips were not included in the analysis. The engineering stress-strain relationship obtained based on the crosshead displacement and the force measured by the load cell are shown in Figure 6.

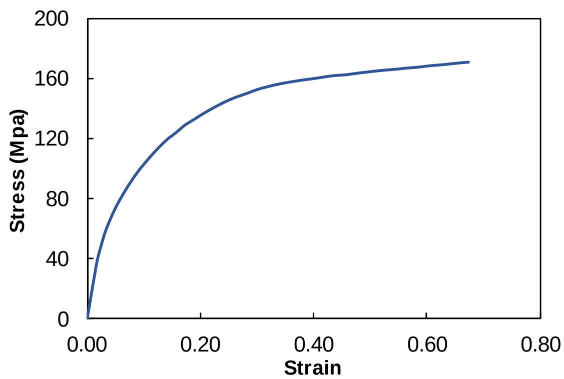


**Figure 6 Uniaxial tensile test of Kapton HPP-ST, conducted at ambient conditions and a strain rate of 0.002 s$^{-1}$.**

### 3.1.2. Equi-biaxial test

Due to the maximum load limit of the biaxial-test bench and the minimum sample size, the highest obtained strain was 16%. However, the applied strain in the characterization test is about 4%. Therefore, this amount of strain was deemed adequate to parameterize the constitutive model. Three specimens were tested, and the average results are shown in Figure 7. Because of the isotropic behavior of the Kapton, the stress-strain results in both stretching directions was nearly identical.

## 2.4 Hyperelastic Model

Uniaxial and Equi-biaxial experimental results were used to calibrate the constitutive model and reproduce the material behavior in finite element model. For a hyperelastic model, material is considered to undergo large strain, with the stress determined by the current state of deformation (not path-dependence). This allows the determination of the internal strain energy. The stress-strain relationship may now be derived for any load path, as the stress is the derivative of the strain energy density function with respect to its conjugate strain quantity. The strain energy density may be fitted to a number of functional forms based on constitutive models introduced in the literature. The constants of such a function are calibrated using the measured experimental values.

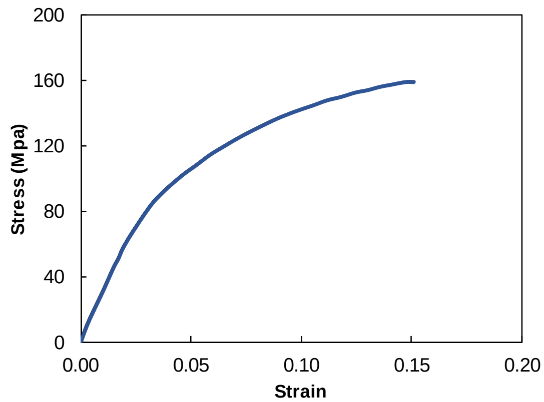


**Figure 7 Equi-biaxial test result of Kapton HPP-ST test conducted at ambient condition and strain rate of 0.002 $s^{-1}$ in both directions.**

The strain energy density for an isotropic material may only be function of the three deviatoric invariants of the right Cauchy-Green deformation tensor, **C**, (or any other relevant strain quantitie). It was assumed that the material is incompressible, which leads to a constant Jacobian determinant of *J=1*. The deviatoric portion of the energy is only a function of

$$\bar{I}_1 = \bar{\lambda}_1^2 + \bar{\lambda}_2^2 + \bar{\lambda}_3^2, \tag{1}$$

$$\bar{I}_2 = \bar{\lambda}_1^2\bar{\lambda}_2^2 + \bar{\lambda}_2^2\bar{\lambda}_3^2 + \bar{\lambda}_3^2\bar{\lambda}_1^2, \tag{2}$$

where $\bar{\lambda}_i$ are the deviatoric eigenvalues of tensor **C** or the deviatoric stretches. Note that in volume preserving deformations the third invariant of the tensor **C**, is identically $I_3=1$, and the deviatoric invariants are simply equal to the total invariants since *J=1*.

For either test results, the strain energy density was obtained by integrating the stress-strain data and were plotted with respect to the first invariant, $U = U_1(I_1)$, as shown in Figure 8. The fact that both uniaxail and equi-biaxail energies match in this figure supports the choice to drop the dependence on the second invariant $I_2$. Further testing has shown that some of the nonlinearity in the tensile response is due to inelastic deformations, but this was not included in the present study.

Abaqus provides a number of model for hyperelastic materials that may be checked for best fit. The Marlow model (for incompressible materials) is essentially a general function of the first deviatoric invarinat. The fitting results of the Marlow model and other well-known models for both uniaxial and Equi-biaxial are shown in Figure 9. It appears that among all these choices, the free-functional form of the Marlow model is most successful in matching the experimental data and particularly the pronounced softening observed in experiment. However, as stated earlier, this softening behavior might be due to plastic yielding of the specimen and needs further study. The Marlow model assumes that the strain energy density is only a function of first deviatoric invariant which agrees well with our observations above. Mooney-Rivlin and Arruda-Boyce models appear unable to reconcile the observed responses in uniaxial and equi-biaxial tests and Van-Der-Waals model shows a significant hardening in the equi-biaxial response that is not present in the experiment.

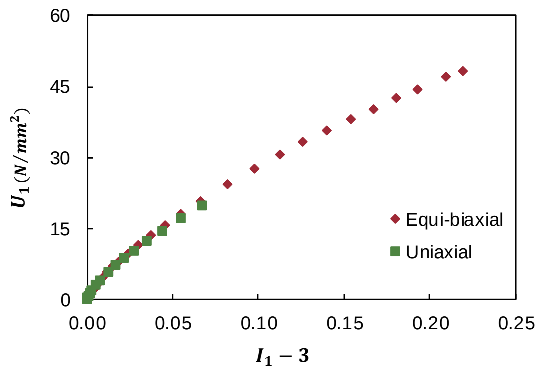


**Figure 8 Strain energy density obtained by integrating the uniaxial and equi-biaxial stress-strain data.**

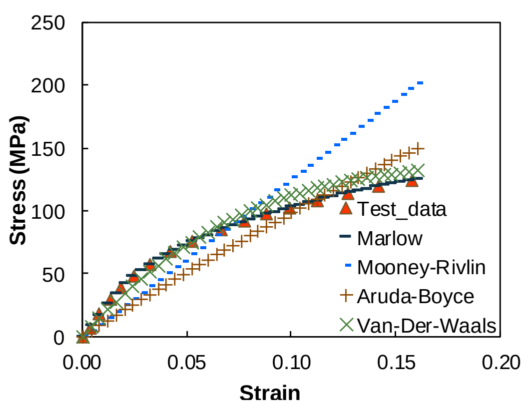


a)

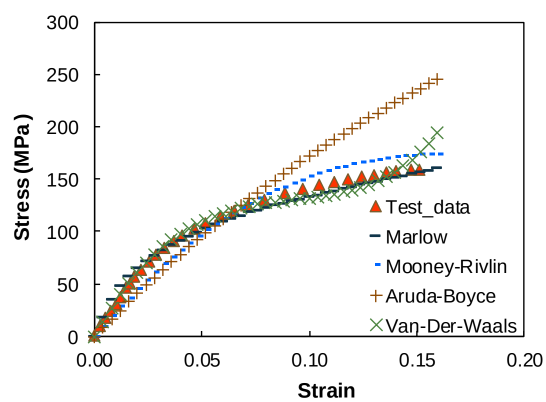


b)

**Figure 9 Various material models fit to a) Uniaxial test data and b) Equi-biaxial test data. The Marlow model appears to be the most accurate constitutive model for this material.**

## 2.5 Parametric Study of Loading

The first goal of the parametric study is to design an experiment to characterize the interface properties of FHEs by capturing failure for different mixed-mode ratios. By obtaining different mixed-mode ratios and fitting the results, the traction separation parameters for pure mode I and mode II can be extrapolated. The parameters will be used in finite element models in the future and the failure mechanism of the FHEs under different loading configuration will be predicted. In turn, the results will enable the manufacturer to improve their design.

To design the characterization experiment, a nonlinear study was performed using a simple model as illustrated in Figure 2. The virtual specimen was subjected to axial and transverse tensile loading only. The stress ratio was measured at the contact tip.

The axial displacement was set at 1.5 mm while the transverse displacement component was varied from 0 to 0.15 mm, causing the displacement ratio, $u_2/u_1$ , to vary from 0 to 0.1 by a 0.01 step. The resulting mixed-mode ratios are plotted in Figure 10. As shown, by increasing the transverse displacement, the mixed-mode ratio decreased, which is because of the reduction in the normal stress. The negative mixed-mode ratio indicates that the normal stress is in compressive mode.

Additionally, the model fully captured the effects of material nonlinearity. A small drop in mixed mode ratio, which is indicated on the plot, is when the silver paste started plastic deformation. The most important outcome of this study is that different mixed-mode ratios can be obtained by altering the loading conditions. Therefore, by considering the axial displacement as a linear ramp function, a constant mixed-mode ratio can be obtained by adjusting the transverse displacement nonlinearly by following a constant mixed-mode ratio in Figure 10. The $u_2$ function can be divided into two parts: the first part is an almost linear function defined before silver paste yielding. Subsequently, since since the post-yield deformation of the silver paste is modeled as nearly volume preserving, the transverse displacement will be defined as a nonlinear descending function.

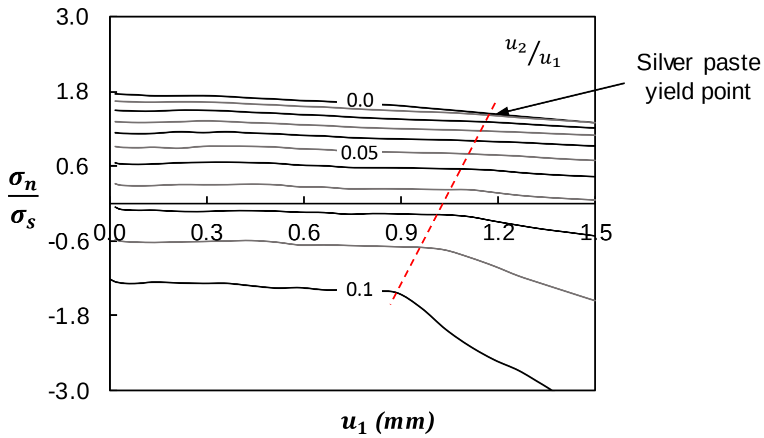


**Figure 10 Effects of different transverse to axial displacement ratio ($u_2/u_1$) on the mixed-mode ratio which defined as $\sigma_n/\sigma_s$**

## 3. Conclusion

A parametric study, based on a detailed finite element analysis with cohesive zone modeling, has been performed on a proposed sample design that allows different mode I to mode II loading ratios. The results constitute the basis of testing method, in which small modification of independently applied axial and transverse displacements produced desired mixed mode ratios. The model accounted for nonlinear material behavior and geometric effects. The substrate was modeled as a hyperelastic material. Uniaxial and equi-biaxial tensile tests were performed to fit a phenomenological constitutive model. To investigate the effects of loading on the mixed-mode ratio, the model was subjected to biaxial applied displacement paths. The transverse displacements were varied, and the resulted mixed-mode ratio, defined as $\sigma_n/\sigma_s$ , at contact tip was determined numerically. It was shown that the mixed-mode ratio is sensitive to the transverse displacement. The normal stress was decreased as the transverse compressive displacement was increased. Therefore, this model will allow designing efficient experiments to extract traction separation relations for a large range of mixed-mode and pure mode II. Moreover, a nonlinear function for the transverse displacement can be found which yields a constant mixed-mode ratio that can be employed in experiments based on these numerical results. The model can be applied not only to hyperelastic materials, but also materials with other mechanical properties and different thicknesses. Additionally, the range of the predicted mixed-mode ratio by the model is large enough to fully characterize the interface, although, it cannot predict the traction-separation for a pure mode I. The estimation of mode I cohesive zone parameters will require extrapolation of the results obtained in this method. In practice, characterizing the interface will result in predicting the failure mechanisms of FHEs under different loading configurations to speed up device design iterations and improve FHE reliability under large-deformation use.

## 4. Acknowledgment

This material is based, in part, on research sponsored by Air Force Research Laboratory under agreement number FA8650-15-2-5401, as conducted through the flexible hybrid electronics manufacturing innovation institute, NextFlex. The U.S. Government is authorized to reproduce and distribute reprints for Governmental purposes notwithstanding any copyright notation thereon. The views and conclusions contained herein are those of the authors and should not be interpreted as necessarily representing the official policies or endorsements, either expressed or implied, of Air Force Research Laboratory or the U.S. Government.

## 5. References

Abaqus Analysis User’s Guide (2016) [WWW Document], n.d. URL http://abaqus.software.polimi.it/v2016/books/usb/default.htm?startat=pt09.html (accessed 2.21.18).

ASTMD882, 2012.

Barenblatt, G.I., 1962. The mathematical theory of equilibrium cracks in brittle fracture, in: Advances in Applied Mechanics. Elsevier, pp. 55–129.
Benzeggagh, M.L., Kenane, M., 1996. Measurement of mixed-mode delamination fracture toughness of unidirectional glass/epoxy composites with mixed-mode bending apparatus. Compos. Sci. Technol. 56, 439–449. https://doi.org/10.1016/0266-3538(96)00005-X
Cao, Z., Tao, L., Akinwande, D., Huang, R., Liechti, K.M., 2016. Mixed-mode traction-separation relations between graphene and copper by blister tests. Int. J. Solids Struct. 84, 147–159. https://doi.org/10.1016/j.ijsolstr.2016.01.023
Dagdeviren, C., Yang, B.D., Su, Y., Tran, P.L., Joe, P., Anderson, E., Xia, J., Doraiswamy, V., Dehdashti, B., Feng, X., Lu, B., Poston, R., Khalpey, Z., Ghaffari, R., Huang, Y., Slepian, M.J., Rogers, J.A., 2014. Conformal piezoelectric energy harvesting and storage from motions of the heart, lung, and diaphragm. Proc. Natl. Acad. Sci. 111, 1927–1932. https://doi.org/10.1073/pnas.1317233111
Dugdale, D.S., 1960. Yielding of steel sheets containing slits. J. Mech. Phys. Solids 8, 100–104. https://doi.org/10.1016/0022-5096(60)90013-2
Harris, K.D., Elias, A.L., Chung, H.-J., 2016. Flexible electronics under strain: a review of mechanical characterization and durability enhancement strategies. J. Mater. Sci. 51, 2771–2805. https://doi.org/10.1007/s10853-015-9643-3
Hutchinson, J. W., Suo, Z., 1991. Mixed Mode Cracking in Layered Materials, in: Hutchinson, John W., Wu, T.Y. (Eds.), Advances in Applied Mechanics. Elsevier, pp. 63–191. https://doi.org/10.1016/S0065-2156(08)70164-9
Kanninen, M.F., 1973. An augmented double cantilever beam model for studying crack propagation and arrest. Int. J. Fract. 9, 83–92.
Kim, D.-H., Lu, N., Huang, Y., Rogers, J.A., 2012. Materials for stretchable electronics in bioinspired and biointegrated devices. MRS Bull. 37, 226–235.
Leenen, M.A.M., Arning, V., Thiem, H., Steiger, J., Anselmann, R., 2009. Printable electronics: flexibility for the future. Phys. Status Solidi A 206, 588–597. https://doi.org/10.1002/pssa.200824428
Li, S., Thouless, M.D., Waas, A.M., Schroeder, J.A., Zavattieri, P.D., 2006. Mixed-mode cohesive-zone models for fracture of an adhesively bonded polymer–matrix composite. Eng. Fract. Mech. 73, 64–78. https://doi.org/10.1016/j.engfracmech.2005.07.004
Li, S., Thouless, M.D., Waas, A.M., Schroeder, J.A., Zavattieri, P.D., 2005. Use of mode-I cohesive-zone models to describe the fracture of an adhesively-bonded polymer-matrix composite. Compos. Sci. Technol. 65, 281–293. https://doi.org/10.1016/j.compscitech.2004.07.009
Mu, Q., Dunn, C.K., Wang, L., Dunn, M.L., Qi, H.J., Wang, T., 2017. Thermal cure effects on electromechanical properties of conductive wires by direct ink write for 4D printing and soft machines. Smart Mater. Struct. 26, 045008. https://doi.org/10.1088/1361-665X/aa5cca
Najafian, S., Amirkhizi, A.V., Stapleton, S., 2018. Interfacial characterization of flexible hybrid electronics, in: Behavior and Mechanics of Multifunctional Materials and Composites XII. Presented at the Behavior and Mechanics of Multifunctional Materials and Composites XII, International Society for Optics and Photonics, p. 105961T. https://doi.org/10.1117/12.2312103

Park, S.-I., Ahn, J.-H., Feng, X., Wang, S., Huang, Y., Rogers, J.A., 2008. Theoretical and experimental studies of bending of inorganic electronic materials on plastic substrates. Adv. Funct. Mater. 18, 2673–2684.
Suo, Z., Hutchinson, J.W., 1990. Interface crack between two elastic layers. Int. J. Fract. 43, 1–18. https://doi.org/10.1007/BF00018123
Van Der Sluis, O., Hsu, Y.-Y., Timmermans, P.H.M., Gonzalez, M., Hoefnagels, J.P.M., 2010. Stretching-induced interconnect delamination in stretchable electronic circuits. J. Phys. Appl. Phys. 44, 034008.
Williams, 1959. The stresses around a fault or crack in dissimilar media. Bull. Seismol. Soc. Am. 49, 199–204.
Williams, J.G., 1989. End corrections for orthotropic DCB specimens. Compos. Sci. Technol. 35, 367–376. https://doi.org/10.1016/0266-3538(89)90058-4
Wu, C., Gowrishankar, S., Huang, R., Liechti, K.M., 2016. On determining mixed-mode traction–separation relations for interfaces. Int. J. Fract. 202, 1–19. https://doi.org/10.1007/s10704-016-0128-4
Wu, C., Huang, R., Liechti, K.M., 2017. Characterizing Interfacial Sliding of Through-Silicon-Via by Nano-Indentation. IEEE Trans. Device Mater. Reliab. 17, 355–363. https://doi.org/10.1109/TDMR.2017.2681580